ELSEVIER

Applied Surface Science 96–98 (1996) 24–32

applied surface science

# An analytical model for three-dimensional laser plume expansion into vacuum in hydrodynamic regime

S.I. Anisimov [a,*], B.S. Luk'yanchuk [b], A. Luches [c]

[a] *L.D. Landau Institute for Theoretical Physics, Russian Academy of Sciences, 117940 Moscow, Russia*
[b] *General Physics Institute, Russian Academy of Sciences, 117942 Moscow, Russia*
[c] *Department of Physics, University of Lecce, 73100 Lecce, Italy*

Received 22 May 1995

**Abstract**

Dynamic of a dense, laser-produced vapor plume is studied. The analysis is based on the special solution of gas dynamics equations that describes the expansion of an ellipsoidal gas cloud into vacuum. This solution is employed to explain the apparent 'rotation' of the cloud — the so called 'flip-over effect'. The flux of atoms onto the substrate and the film thickness profile are calculated using the model. The present model can be used for the interpretation of the time-of-flight spectra of atoms in laser ablation, and for the description of the shape of vapor cloud expanding into an ambient gas.

## 1. Introduction

Pulsed laser deposition (PLD) is extensively employed for the growth of thin films. This method is used to grow high-$T_c$ superconducting thin films, multi-layer X-ray mirrors, diamond-like carbon films, etc. (see reviews [1–6]). The films produced by PLD are nonuniform in thickness. The thickness profile is determined by the angular distribution of the mass flux of evaporated material which, in turn, depends on the evaporation regime and on the focal spot shape. This has been studied in detail both theoretically and experimentally [7–18]. Note that, in the major part of theoretical studies, vapour expansion is assumed to be isothermal. This assumption is not confirmed by the experiment [19–21] and numerical calculations (e.g., [22]). Adiabatic expansion of a non-isothermal plume was studied in [17]. However, the analysis [17] is restricted to the case of axially-symmetric flow, which is relevant for the circular focal spots. Experimentally, non-circular spots are of considerable use, so that the vapor flow has, generally, no axial symmetry. It should be noted that the initial asymmetry of vapor cloud is not 'forgotten' during its expansion. To the contrary, the asymptotic shape of the expanding cloud is determined just by this initial asymmetry. For example, the experiments [9,12,13] reveal that, for an elliptic focal spot, the spot of deposited material has elliptic shape with the axes rotated by 90° (so called 'flip-over effect'). Clearly such effects can not be understood on the basis of axially-symmetric model.

The spatial structure of the vapor plume produced by nanosecond laser pulse is well known since the

* Corresponding author.


*SSDI* 0169-4332(95)00373-8

60th. It was shown [19] that a dense cloud ($n \geq 10^{21}$ $cm^{-3}$) of the evaporated material is formed in the immediate vicinity of the target. Maximum velocity of the outer boundary of this cloud is about $10^6$ cm/s (for carbon at the laser intensity $10^9$ W/cm$^2$). The size of the cloud grows during the laser pulse due to material evaporation and saturates for typical times by order of 1–3 durations of laser pulse. For the laser intensities higher $4 \cdot 10^7$ W/cm$^2$ the boundary of the dense cloud even slowly collapsed towards the center after the laser pulse end.

In the present paper, we study the three-dimensional expansion of the dense core of laser plume. We use the special solution of gas dynamics equations describing the motion of gas with uniform deformation. This solution results from the Lie group invariance properties of the gas dynamics equations [23,24]. One-dimensional solutions of this type were first studied in [25]. Three-dimensional uniform deformation solutions were first considered in [26]. It was shown that the gas dynamics equations can be reduced to the set of equations of motion of a point in nine-dimensional space. The same result was obtained later in [27]. In specific cases, the set of ordinary differential equations derived in [25,26] was solved numerically [27–29], or analytically [30]. Qualitative analysis of these equations was performed in [31].

Special solutions of gas dynamics equations obtained in [26] allow for an arbitrary initial temperature profile. Recently, simplest solutions of this type with constant temperature were employed for the interpretation of experimental results on laser ablation (see, e.g., [10,11,14]). Note that the isothermal flow model is not reconcilable with experiment and quite often inadequate because, in the framework of hydrodynamics, there is no physical mechanism to maintain a finite temperature at the boundary of expanding cloud. We assume that the temperature at the cloud boundary is zero. This is the case, in particular, for uniform initial entropy distribution over a cloud [17]. Some of the results obtained in this paper are quite general and do not depend on a particular initial entropy profile. However, a number of cloud characteristics are sensitive to the initial conditions, so that appropriate experiments can give an information about the initial state of evaporated material.

## 2. Model

The schematic of typical PLD-experiment is shown in Fig. 1. The laser beam with a pulse length of about few tens of nanoseconds produces a vapor cloud near the target surface located at $z = 0$. The cloud expands into vacuum and reaches the substrate located at $z = z_s$ at time $t_s$, which is of the order of $z_s/c_s$, $c_s$ being the sound speed. We assume that the formation time of the initial cloud is much shorter than the time of its expansion. The expansion of the vapor cloud is described by the gas dynamics equations

$$\frac{\partial \rho}{\partial t} + \mathrm{div}(\rho \boldsymbol{v}) = 0, \tag{1}$$

$$\frac{\partial \boldsymbol{v}}{\partial t} + (\boldsymbol{v}\nabla)\boldsymbol{v} + \frac{1}{\rho}\nabla p = 0, \tag{2}$$

$$\frac{\partial S}{\partial t} + (\boldsymbol{v}\nabla)S = 0, \tag{3}$$

where $\rho$, $p$, $\boldsymbol{v}$ and $S$ are the density, pressure, velocity, and entropy (per unit mass), respectively. We consider the vapor as an ideal gas with a constant adiabatic index $\gamma = c_p/c_v$.

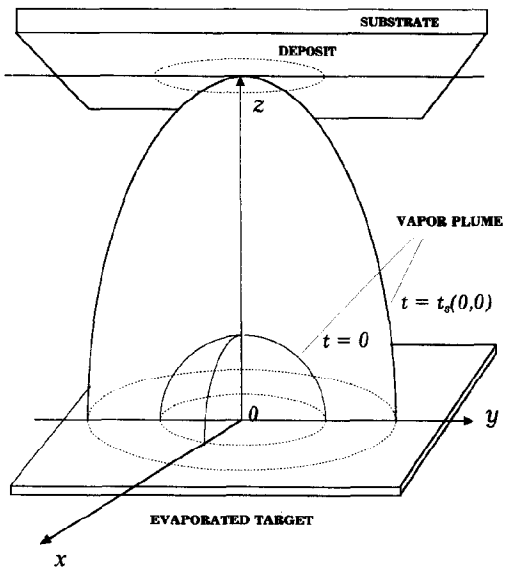


Fig. 1. The schematic of typical PLD-experiment. The shape of expanding vapor cloud is shown for two moments of time $t = 0$ and $t = t_s(0, 0)$.

As pointed out above, a special solution of the gas dynamics equations (1)–(3) obtained in [25] is employed for the analysis of vapor expansion. With this solution, the flow parameters are constant at ellipsoidal surfaces. The coordinates of a fluid particle $r_i(t)$ change with time according to the affine transformation

$$r_i(t) = F_{ik}(t)\, a_k, \quad i,k = x, y, z, \tag{4}$$

where $a_k = r_k(0)$ are the Lagrangian coordinates of the particle and summation is carried out over recurring subscripts. For present purposes, it is sufficient to consider a non-spinning cloud. In this case, the matrix $F_{ik}(t)$ has diagonal form:

$$F_{ik} = \begin{vmatrix} X(t)/X_0 & 0 & 0 \\ 0 & Y(t)/Y_0 & 0 \\ 0 & 0 & Z(t)/Z_0 \end{vmatrix}, \tag{5}$$

where $X_0$, $Y_0$, $Z_0$ are the initial values of $X(t)$, $Y(t)$, $Z(t)$, respectively. One can see from Eq. (4) that gas particle velocity is a linear function of its radius-vector:

$$v_i = \dot{F}_{ik} F_{kj}^{-1} r_j \tag{6}$$

where $F_{kj}^{-1}$ is inverse of matrix $F_{kj}$. Substituting (4) into (1)–(3), we arrive at a set of ordinary differential equations, provided the density and pressure profiles have the following forms:

$$p(\boldsymbol{r}, t) = h(t)\, H(\chi), \qquad \rho(\boldsymbol{r}, t) = f(t)\frac{\mathrm{d}H}{\mathrm{d}\chi},$$

$$f(t) = A_0\left[\det(F_{ij})\right]^{-1}, \quad h(t) = B_0\left[\det(F_{ij})\right]^{-\gamma},$$

$$\chi = g_{ik} a_i a_k, \tag{7}$$

where $A_0$ and $B_0$ are constants and $g_{ik}$ is a constant symmetric matrix.

Taking the matrix $F_{ik}$ in the form (5), the profiles of density and pressure may be written as

$$\rho(\boldsymbol{r}, t) = \frac{M}{I_1(\gamma)\, XYZ}\left[\psi(x, y, z, t)\right]^{\alpha},$$

$$\psi = 1 - \frac{x^2}{X^2} - \frac{y^2}{Y^2} - \frac{z^2}{Z^2},$$

$$p(\boldsymbol{r}, t) = \frac{E}{I_2(\gamma)\, XYZ}\left[\frac{X_0 Y_0 Z_0}{XYZ}\right]^{\gamma-1} \times \left[\psi(x, y, z, t)\right]^{\alpha+1}. \tag{8}$$

Here $M = \int \rho(\boldsymbol{r}, t)\,\mathrm{d}V$ is the mass and $E = (\gamma - 1)^{-1}\int p(\boldsymbol{r}, 0)\,\mathrm{d}V$ is the initial energy of the vapor cloud. The constants $I_1$, $I_2$ appearing in Eq. (8) are equal to

$$I_1(\gamma) = \frac{\pi^{3/2}}{2}\frac{\Gamma(\alpha+1)}{\Gamma\left(\alpha+\frac{5}{2}\right)},$$

$$I_2(\gamma) = \frac{\pi^{3/2}}{2(\gamma-1)}\frac{\Gamma(\alpha+2)}{\Gamma\left(\alpha+\frac{7}{2}\right)},$$

where $\Gamma(z)$ is the Gamma-function. For the density and pressure profiles defined by Eq. (8), the entropy depends on the coordinates and time as

$$S = \frac{1}{\gamma-1}\ln\left\{\frac{E}{X_0 Y_0 Z_0 I_2}\left(\frac{X_0 Y_0 Z_0 I_1}{M}\right)^{\gamma} \times \left[\psi(x, y, z, t)\right]^{1-\alpha(\gamma-1)}\right\} + \text{const.} \tag{9}$$

The entropy remains constant at the moving ellipsoidal surfaces $\psi(x, y, z, t) = \text{const}$. The entropy gradient is directed outward if $\alpha(\gamma - 1) > 1$ and inward if $\alpha(\gamma - 1) < 1$. When the initial vapor cloud is isentropic, $\alpha = 1/(\gamma - 1)$.

Using Eqs. (5), (6), (8), the gas dynamics equations (1)–(3) can be reduced to a set of ordinary differential equations for the elements of matrix $F_{ik}$

$$\ddot{X} = -\frac{\partial U}{\partial X}, \quad \ddot{Y} = -\frac{\partial U}{\partial Y}, \quad \ddot{Z} = -\frac{\partial U}{\partial Z}, \tag{10}$$

where

$$U = \frac{5\gamma - 3}{\gamma - 1}\frac{E}{M}\left[\frac{X_0 Y_0 Z_0}{XYZ}\right]^{\gamma-1}.$$

The equations (10) are identical with the equations of motion of a point particle in three-dimensional Euclidean space. The initial conditions for Eq. (10) are taken in the form

$$X(0) = X_0, \quad Y(0) = Y_0, \quad Z(0) = Z_0,$$

$$\dot{X}(0) = \dot{Y}(0) = \dot{Z}(0) = 0. \tag{11}$$

Here we assume for simplicity that the initial kinetic energy of the vapor is much smaller than its internal energy. This assumption may be subject to refinement when more detailed information on the initial vapor cloud is available.

Except of some special cases, Eq. (10) are not completely integratable in terms of known functions. An example of analytical solution of these equations, for the special case $\gamma = \frac{5}{3}$, is given in reference [30]. In general, Eq. (10) can be integrated numerically. For this purpose, we transform Eq. (10) to dimensionless form using $X_0$ as a spatial scale length:

$$\xi\ddot{\xi} = \eta\ddot{\eta} = \zeta\ddot{\zeta} = \left[\frac{\eta_0\zeta_0}{\xi\eta\zeta}\right]^{\gamma-1} \tag{12}$$

with initial conditions

$$\xi(0) = 1, \quad \eta(0) = \eta_0, \quad \zeta(0) = \zeta_0,$$
$$\dot{\xi}(0) = \dot{\xi}(0) = \dot{\xi}(0) = 0, \tag{13}$$

where

$$\xi = X/X_0, \quad \eta = Y/X_0, \quad \zeta = Z/X_0,$$
$$\tau = t\beta^{1/2}/X_0, \quad \eta_0 = Y_0/X_0,$$
$$\zeta_0 = Z_0/X_0, \quad \beta = (5\gamma - 3)\frac{E}{M}. \tag{14}$$

Without loss of generality, the axes of the initial ellipsoid can be chosen in such a way that $X_0 \geq Y_0 \geq Z_0$. We have, therefore, $\zeta_0 \leq \eta_0 \leq 1$. The energy integral follows immediately from Eq. (12)

$$\tfrac{1}{2}\left(\dot{\xi}^2 + \dot{\eta}^2 + \dot{\zeta}^2\right) + \frac{U(\tau)}{\beta} = \varepsilon = (\gamma - 1)^{-1} = \text{const.} \tag{15}$$

In the special case $\gamma = \frac{5}{3}$ Eq. (12) has an additional integral [30]:

$$\xi^2 + \eta^2 + \zeta^2 = 3\tau^2 + 1 + \eta_0^2 + \zeta_0^2. \tag{16}$$

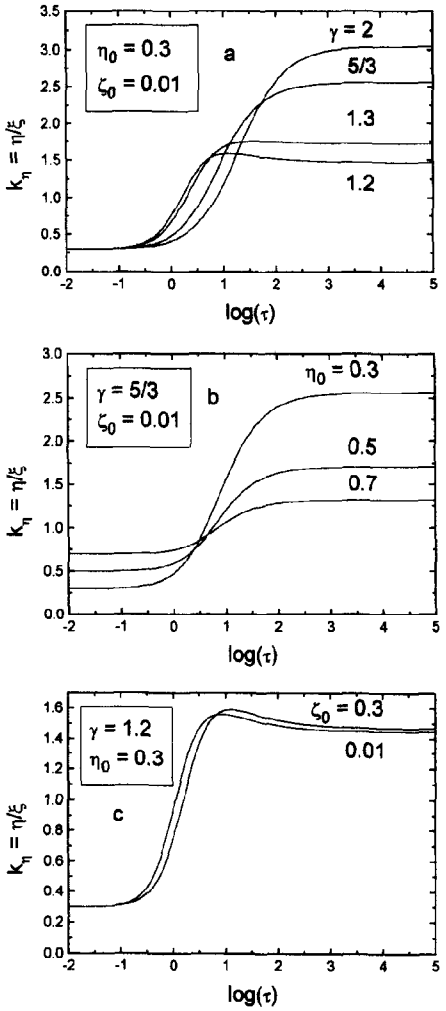


Fig. 2. Dependencies of $k_\eta(\tau)$.

## 3. Numerical integration. Flip-over-effect

One can see from (12) and (13) that the vapor flow is determined by three parameters: $\eta_0$, $\zeta_0$, and $\gamma$. The set of equations (12) was solved numerically for whole range of these parameters associated with laser ablation. It is evident that the vapor expansion becomes inertial when $\tau \to \infty$. We introduce the new functions $k_\eta(\tau) = \eta(\tau)/\xi(\tau)$ and $k_\zeta(\tau) = \zeta(\tau)/\xi(\tau)$, describing time variations of the shape of expanding vapor cloud. Figs. 2 and 3 show typical dependencies $k_\eta(\tau)$ and $k_\zeta(\tau)$ for different values of parameters $\gamma$, $\eta_0$ and $\zeta_0$. Note that $k_\eta(\tau)$, $k_\zeta(\tau)$ are monotonically increasing functions of time for $\gamma \geq \frac{5}{3}$ and reach their asymptotic values, $k_\eta(\infty)$ and $k_\zeta(\infty)$, respectively, at $\tau$ of the order of $10^3$. For $\gamma < \frac{5}{3}$ the functions $k_\eta(\tau)$, $k_\zeta(\tau)$ reach their maximum values at finite $\tau$ and then slowly decrease.

As shown in Fig. 2, the function $k_\eta(\tau)$ reaches the value $k_\eta = 1$ at $\tau \approx 10$. At this point the plume becomes symmetric about $z$-axis. At a later time, $k_\eta(\tau)$ continues to grow, hence $\eta(\tau) > \xi(\tau)$ at large $\tau$. We see, thus, that the expansion of an ellipsoidal cloud goes faster along the axis that initially was

shorter. This explains apparent 'rotation' of laser plume during its expansion observed experimentally in references [9,12,13]. It is obvious, that a similar effect will take place for an arbitrary focal spot with the axis of rotation of $n$-th order, $C_n$. In this case the angle of rotation is equal to $\pi/n$.

An analysis shows that $k_\eta(\tau)$ depends strongly on the parameter $\eta_0$ and practically does not depend on the parameter $\zeta_0$, whereas $k_\zeta(\tau)$ has strong dependence on $\zeta_0$ and only week dependence on $\eta_0$. One can say that the plume expansion resembles a superposition of two independent motions: (1) the expansion along the $z$-axis controlled mainly by the parameter $\zeta_0$, and (2) the expansion in the $(xy)$-plane largely dependent on the parameter $\eta_0$. If $\gamma$ is not close to unity, both motions become inertial at $\tau$ on the order of 100 to 1000. Since this moment, the shape of the cloud does not change, and the functions $k_\eta(\tau)$ and $k_\zeta(\tau)$ take their asymptotic values, $k_\eta(\infty)$ and $k_\zeta(\infty)$, respectively. Some of these values are presented in Tables 1 and 2.

## 4. Time-of-flight spectra

In order to investigate the structure and dynamics of laser produced vapor plumes, the time-of-flight (TOF) mass spectroscopy is widely used. Measured TOF distributions can be employed, in principle, to determine parameters of the initial vapor cloud. When the mass of vapor is small, the cloud expands in free-molecular (collisionless) regime, and TOF distribution can readily be expressed in terms of the initial velocity distribution of evaporated atoms. This simplest approach cannot be applied, however, when the plume expands in hydrodynamic regime. In this case, the solution of gas dynamics equations considered in the present paper offers a proper basis for the analysis of TOF spectra. In Fig. 4, the time dependence of the vapor density at the point $\xi_m = 0$, $\eta_m = 0$, $\zeta_m = 10$ is shown by circles. The calculation was performed using Eq. (8) with $\gamma = 1.1$, $\alpha = 10$. The curve presented in Fig. 4 is similar to experimentally measured TOF distributions (see, e.g., [14,32–35]).

Notice that the dependence shown in Fig. 4 can be approximated by the Gaussian function (solid line in Fig. 4):

$$\rho_m(\tau) = \frac{A}{\tau^3}\exp\left[-B\left(\frac{z}{\tau} - u\right)^2\right], \qquad (17)$$

where $A$, $B$, and u are constants. Functions of this type were used in [14,32] to describe TOF spectra, and the adjustable parameter $B$ was related to an

Table 1
$k_\zeta = k_\zeta(\zeta_0, \gamma)$

| | $\zeta_0$ | | | | | | |
|---|---|---|---|---|---|---|---|
| $\gamma$ | 0.001 | 0.003 | 0.01 | 0.03 | 0.1 | 0.3 | $\eta_0$ |
| 1.1 | 2.16 | 1.97 | 1.77 | 1.59 | 1.39 | 1.20 | 1.0 |
| | 2.28 | 2.08 | 1.86 | 1.66 | 1.43 | 1.22 | 0.3 |
| | 2.40 | 2.18 | 1.93 | 1.71 | 1.45 | 1.22 | 0.1 |
| 1.2 | 3.69 | 3.18 | 2.67 | 2.24 | 1.79 | 1.39 | |
| | 4.21 | 3.61 | 3.00 | 2.48 | 1.92 | 1.44 | |
| | 4.81 | 4.09 | 3.35 | 2.70 | 2.02 | 1.47 | |
| 1.3 | 6.00 | 4.84 | 3.78 | 2.96 | 2.17 | 1.55 | |
| | 7.26 | 5.83 | 4.50 | 3.45 | 2.44 | 1.65 | |
| | 9.07 | 7.21 | 5.45 | 4.03 | 2.68 | 1.71 | |
| 1.4 | 9.66 | 7.23 | 5.20 | 3.77 | 2.55 | 1.69 | |
| | 12.2 | 9.09 | 6.46 | 4.58 | 2.96 | 1.83 | |
| | 16.4 | 12.1 | 8.40 | 5.69 | 3.38 | 1.93 | |
| 5/3 | 35.8 | 20.7 | 11.3 | 6.52 | 3.53 | 1.98 | |
| | 45.9 | 24.4 | 14.4 | 8.16 | 4.24 | 2.21 | |
| | 65.6 | 37.6 | 20.1 | 10.9 | 5.15 | 2.40 | |

The three numbers in each block demonstrate the dependence of $k_\zeta$ on parameter $\eta_0$.

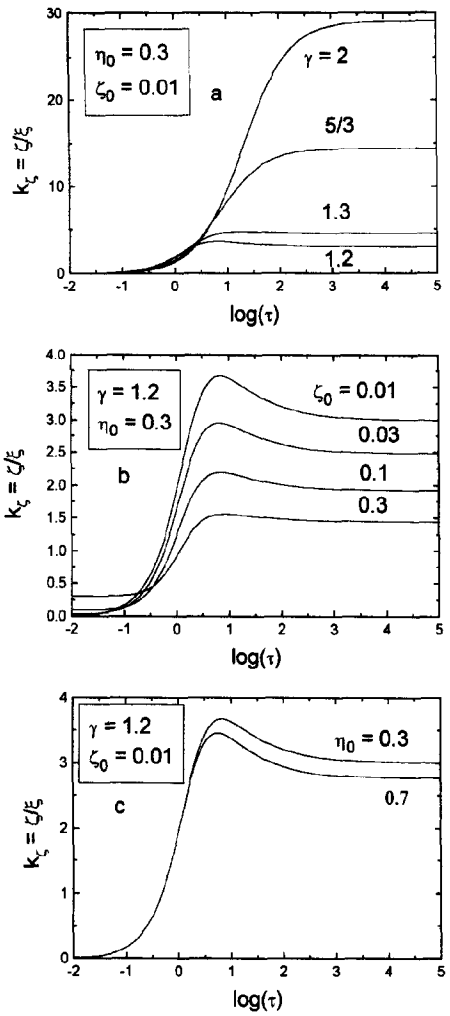


Fig. 3. Dependencies of $k_\zeta(\tau)$.

'effective temperature' of the vapor. This approach is not justified, because the 'effective temperature', thus defined, does not exhibit the properties of thermodynamic temperature (it depends, for example, on the shape of initial vapor cloud).

## 5. Expansion of vapor cloud into an ambient gas

So far it has been assumed that the evaporated material expands into vacuum. The presence of an ambient gas complicates the situation. The evaporated material acts on the surrounding gas like a piston generating a shock wave in the gas. The shock-compressed gas is separated from the expanding vapor by the contact surface, whose velocity slows down with time. As the result of contact surface deceleration, an additional shock wave arises in the vapor. The flow structure outlined above is

Table 2
$k_\eta = k_\eta(\eta_0, \gamma)$

| | $\eta_0$ | | | |
|---|---|---|---|---|
| $\gamma$ | 1 | 0.3 | 0.1 | 0.03 | $\zeta_0$ |
| 1.1 | 1 | 1.22 | 1.44 | 1.72 | $10^{-3}$ |
| | | 1.22 | 1.45 | 1.73 | $10^{-2}$ |
| | | 1.22 | 1.45 | 1.71 | $10^{-1}$ |
| 1.2 | 1 | 1.46 | 2.03 | 2.87 | |
| | | 1.47 | 2.05 | 2.91 | |
| | | 1.47 | 2.02 | 2.70 | |
| 1.3 | 1 | 1.71 | 2.78 | 4.74 | |
| | | 1.72 | 2.81 | 4.76 | |
| | | 1.71 | 2.68 | 4.03 | |
| 1.4 | 1 | 1.95 | 3.68 | 7.65 | |
| | | 1.96 | 3.72 | 7.52 | |
| | | 1.93 | 3.38 | 5.69 | |
| 5/3 | 1 | 2.58 | 6.53 | 19.4 | |
| | | 2.56 | 6.33 | 17.4 | |
| | | 2.40 | 5.15 | 10.9 | |

The three numbers in each block demonstrate the dependence of $k_\eta$ on parameter $\zeta_0$.

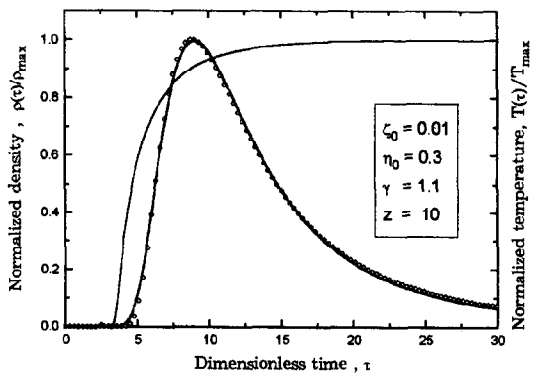


Fig. 4. Density of species according to formula (8) (circles) with $\alpha = 1/(\gamma - 1)$. The solid line is Maxwellian distribution according to (17). The dashed line is hydrodynamical temperature according to $T^\gamma P^{1-\gamma} = \text{const}$.

similar to that occurring when detonation products expand into an ambient gas. As shown in [36], in the flows of this type, the contact surface is unstable. This instability, called the Rayleigh–Taylor instability, results in turbulent mixing between the expanding medium and the ambient gas [37]. These phenomena were observed experimentally in detonation [38,39] and laser ablation [40–42].

In the strict sense, special solution of gas dynamics equations considered in this paper is applicable only to the expansion into vacuum. It can be extended to the expansion into an ambient gas when the gas pressure is low, $P_0 < E/X_0Y_0Z_0$. In this case, the contact surface is described by the equation

$$p(x, y, z, t) = P_0 \tag{18}$$

where $p(x, y, z, t)$ is given by (8). It is easy to show that each point of this surface initially moves away from the origin, and stops at a time $t = t^*(x, y, z)$, when its distance from the origin reaches maximum. The set of thus defined stagnation points forms the surface of stationary vapor plume. The stationary plume can be observed using time-integrated photography [40,43]. The length of the plume in $z$-direction is expressible as

$$L = \left\{1 - \left[\xi(\tau^*)\eta(\tau^*)\zeta(\tau^*)\right]^{(\gamma-1)} \times \left[p_0 I_2(\gamma)\right]^{(\gamma-1)/\gamma}\right\}^{1/2} \zeta(\tau^*) X_0, \tag{19}$$

where $p_0 = P_0 X_0^3 (\eta_0 \zeta_0)^{1-\gamma}/E$. In Fig. 5, the dependence (19) is compared with experimental data [40] where the ablation of high-$T_c$ superconducting material $YBa_2Cu_3O_7$ in the oxygen atmosphere was studied.

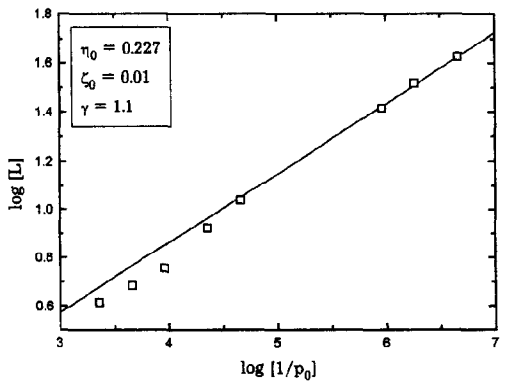


Fig. 5. The normalized plume length $L = L/X_0$ of stationary plume according to (19), obtained from the solution of gas dynamics equations. Squares are experimental data [40].

Within the wide region of the ambient gas pressures the model under consideration predicts the pressure's dependence of the plume length in the form

$$L \approx X_0 G \left[\frac{P_0 X_0^3}{E}\right]^{-\beta} \tag{20}$$

where $G$ and $\beta$ are functions of $\eta_0$, $\zeta_0$, and $\gamma$. The values of $\beta$ which follow from (19) are given in [44]. The analytical solution for the spherical plume yields [40]:

$$G = [3(\gamma-1)]^{1/2} 2^{1/(3(\gamma-1))} (3\gamma-1)^{(1-3\gamma)/(6(\gamma-1))} \times \left[\frac{\pi^{3/2}}{2(\gamma-1)} \frac{\Gamma\left(\frac{\gamma}{\gamma-1}+1\right)}{\Gamma\left(\frac{\gamma}{\gamma-1}+\frac{5}{2}\right)}\right]^{1/(3\gamma)},$$

$$\beta = \frac{1}{3\gamma}.$$

The coefficient $G$ here is smaller (approximately twice for $\gamma = 1.2$) then corresponding coefficient obtained for the rectangular pressure profile [45].

Eq. (20) can be used to determine the adiabatic exponent of ablated material from measured dependence $L(P_0)$. Experimental data [40] give the exponent $\beta = 0.287$. Taking into account that fit depends only slightly on $\eta_0$, $\zeta_0$, and that, $\beta \cong 1/3\gamma$, we obtain: $\gamma = 1.16$. This value is in a good agreement with [34,46].

## 6. Film thickness profile

We now calculate the thickness profile of deposited film, $h(\theta_x, \theta_y)$, where $\theta_x = \arctan(x/z_s)$, $\theta_y = \arctan(y/z_s)$. The mass flux to the substrate surface $z = z_s$ is

$$j(x, y, z_s, t) = \rho(x, y, z_s, t) v_z(x, y, z_s, t) = \begin{cases} \dfrac{M z_s \dot{Z} \psi^{\alpha}}{I_1(\gamma) XYZ^2}, & t \geq t_s(x, y), \\ 0, & t < t_s(x, y). \end{cases} \tag{21}$$

Here $t_s(x, y)$ is the time when the outer boundary of the expanding cloud reaches the substrate $z = z_s$ at the point $(x, y)$ which can be derived from the equation $\psi(x, y, z_s, t_s) = 0$. Integrating the mass flux (21) over the time from $t_s(x, y)$ to infinity and dividing the result by the density of the deposited material $\rho$, we obtain the thickness profile $h(\theta_x, \theta_y)$. In general case, the integration can be performed numerically using the functions $X(t)$, $Y(t)$, $Z(t)$ resulting from numerical solution of (12). A simple analytical expression for $h(\theta_x, \theta_y)$ can be obtained if $z_s \gg X_0$, which is satisfied in many experimental situations. In this case, we can use the asymptotic relations:

$$X(t) = Z(t)/k_\zeta(\infty), \quad Y(t) = Z(t)k_\eta(\infty)/k_\zeta(\infty),$$

and obtain the thickness profile in the form:

$$h(\theta_x, \theta_y) = \frac{Mpq^2}{2\pi\rho_s z_s^2}\left[p + tg^2\theta_x + q^2 tg^2\theta_y\right]^{-3/2}, \tag{22}$$

where $p = 1/k_\zeta(\infty)$ and $q = 1/k_\eta(\infty)$. At small $\theta_x$, $\theta_y$ Eq. (22) is reduced to $h(\theta_x, \theta_y) \propto \cos^m\theta_x \cos^n\theta_y$ with $m = 3/p^2$, $n = 3q^2/p^2$. The values of $m$ and $n$ obtained from numerical integration of Eq. (12) are in agreement with experimental data.

## Acknowledgements

We wish to thank Prof. D. Bäuerle and Dr. N. Arnold for valuable discussions and 'Russian Fund of Fundamental Researches' for financial support. Part of this work was supported also by INTAS-94-902 grant.

## References

[1] S.V. Gaponov, Sov. Phys.-Uspekhi 28 (1985) 522.
[2] D. Bäuerle, Appl. Phys. A 48 (1989) 527.
[3] E.N. Sobol', V.N. Bagratashvili et al., in: Reviews on High-Temperature Superconductivity (Int. Centre of Scient. and Techn. Inform., Moscow, 1990) N3, p. 94
[4] E. Fogarassy and S. Lazare, Eds., Laser Ablation of Electronic materials, Basic Mechanisms and Applications, Proc. E-MRS, Vol. 4 (North-Holland, Amsterdam, 1993).
[5] L.D. Laude, Ed., Excimer Lasers, NATO ASI Series, Vol. E256 (Kluwer, Dordrecht, 1994).
[6] D. Bäuerle, E. Arenholz et al., Mater. Sci. Forum 173/174 (1995) 41.
[7] A.D. Aksakhalian, S.V. Gaponov et al., Zhurn. Tekhn. Fiz. 58 (1988) 1885 (Engl. Trans.: Sov. J. Tech. Phys.).
[8] T. Venkatesan, X.D. Wu et al., Appl. Phys. Lett. 52 (1988) 1193.
[9] R.K. Singh, N. Biuno and J. Narayan, Appl. Phys. Lett. 53 (1988) 1013.
[10] R.K. Singh and J. Narayan, Phys. Rev. B 41 (1990) 8843.
[11] R.K. Singh, O.W. Holland and J. Narayan, J. Appl. Phys. 68 (1990) 233.
[12] C.N. Afonso, R. Serna et al., Appl. Surf. Sci. 46 (1990) 249.
[13] P.E. Muenchausen, K.N. Hubbard et al., Appl. Phys. Lett. 56 (1990) 578.
[14] J.C.L. Kools, T.S. Baller et al., J. Appl. Phys. 69 (1992) 233.
[15] A. Miotello, R. Kelly et al., Appl. Phys. Lett. 61 (1992) 2784.
[16] F. Davanloo, E.M. Juengermann et al., Appl. Phys. A 54 (1992) 369.
[17] S.I. Anisimov, D. Bäuerle and B.S. Luk'yanchuk, Phys. Rev. B 48 (1993) 12076.
[18] R. Kelly and A. Miotello, Nucl. Instr. Meth. Phys. Res. B 91 (1994) 682.
[19] N.G. Basov, V.A. Boyko et al., Sov. Phys.-JETP 24 (1967) 659.
[20] A.D. Aksakhalian, Yu.A. Bityurin et al., Preprint, Institute of Applied Physics, USSR Academy of Sciences (Gorky, 1981).
[21] D.B. Geohegan, Thin Solid Films 220 (1992) 138.
[22] M.K. Matzen and P.L. Morse, Phys. Fluids 22 (1979) 654.
[23] L.V. Ovsyannikov, Group Analysis of Differential Equations (Nauka, Moscow, 1978) (in Russian).
[24] L.V. Ovsyannikov, Lectures on Principles of Gas Dynamics (Nauka, Moscow, 1981) (in Russian).
[25] L.I. Sedov, Dokl. AN SSSR 90 (1953) 735 (in Russian).
[26] L.V. Ovsyannikov, Dokl. AN SSSR 111 (1956) 47 (in Russian).
[27] F.J. Dyson, J. Math. Mech. 18 (1968) 91.
[28] J.M. Dawson, P. Kaw and B. Green, Phys. Fluids 12 (1969) 875.
[29] I.V. Nemchinov, Prikl. Mat. Mekh. 29 (1965) 134 (in Russian).
[30] S.I. Anisimov and Yu.V. Lysikov, J. Appl. Math. Mech. 34 (1970) 882.
[31] O.I. Bogoyavlenskii, Methods of Qualitative Theory of Differential Equations in Astrophysics and Gas Dynamics (Nauka, Moscow, 1980) (in Russian).
[32] H. Nishikawa, M. Kanai et al., Jpn. J. Appl. Phys. 33 (1992) L1090.
[33] J.P. Zheng, Q.Y. Ying et al., Appl. Phys. Lett. 54 (1989) 954.
[34] N.H. Cheung, Q.Y. Ying et al., J. Appl. Phys. 69 (1991) 6349.
[35] R. Kelly and R.W. Dreifus, Nucl. Instr. Meth. Phys. Res. B 32 (1988) 341.
[36] S.I. Anisimov and Ya.B. Zeldovich, Sov. Tech. Phys. Lett. 3 (1977) 445.
[37] S.I. Anisimov, Ya.B. Zeldovich, N.A. Inogamov and M.F.

Ivanov, in: Shock Waves, Explosions, and Detonations, ALAA Prog. in Astron. Aeron. Series, Vol. 87 (1983) p. 218.
[38] A.N. Davydov, E.F. Lebedev et al., Sov. Tech. Phys. Lett. 9 (1983).
[39] A.V. Shurupov, A.N. Davydov et al., Cylindrical Explosion Flows, Preprint N 2-1571, Institute for High Temperatures (USSR Acad. Sci., Moscow, 1985) (in Russian).
[40] E. Stangl, B. Luk'yanchuk et al., in: Excimer Lasers, Ed. L.D. Laude, NATO ASI Series, Vol. E256 (Kluwer, Dordrecht, 1994) p. 79.
[41] K. Scott, J.M. Huntley et al., Appl. Phys. Lett. 57 (1990) 922.
[42] R. Srinivassan, Appl. Phys. A 56 (1993) 417.
[43] S. Proyer and E. Stangl, Appl. Phys. A 60 (1995)
[44] S.I. Anisimov, B.S. Luk'yanchuk and A. Luches, JETP 108 (1995) N7.
[45] P.E. Dyer, A. Issa and P.H. Key, Appl. Phys. Lett. 57 (1990) 186.
[46] R. Kelly and A. Miotello, Appl. Phys. B 57 (1993) 145.